Effects of Chain Length on the Rates of C−C Bond Dissociation in Linear Alkanes and Polyethylene†

Vadim D. Knyazev

Research Center for Chemical Kinetics, Department of Chemistry, The Catholic University of America, Washington, DC 20064, and National Institute of Standards and Technology, Physical and Chemical Properties Division, Gaithersburg, Maryland 20899

Received: September 29, 2006; In Final Form: March 15, 2007

Molecular dynamics modeling of C−C bond dissociation is performed for a series of linear alkanes and polyethylene macromolecules with the chain lengths ranging from one to a thousand constituent ethylene monomers (PE-1−PE-1000). The rate constants obtained in molecular dynamics calculations are compared with those determined using variational transition state theory with the same potential energy surface. The results of simulations demonstrate a significant accelerating effect of chain length on the rates of C−C bond scission. Per-bond rate constant values increase with the increasing chain length, up to an order of magnitude, in the sequence of linear alkanes from PE-1 (ethane) to PE-5 (decane); this dependence becomes saturated for longer chain lengths. Stiffening the potentials of bending and especially the torsional degrees of freedom diminishes the accelerating effect of chain length, while constraining the bond distances for all C−C bonds except the one undergoing dissociation has no effect. The results of the calculations are compared with existing experimental data on the dependences of the rates of thermal decomposition of linear alkanes on the alkane chain length.

1. Introduction

Detailed modeling of the chemical kinetics as a tool of prediction and control of complex chemical processes has achieved great success in the chemistry of many types of gas-phase processes (e.g., combustion, atmospheric modeling) and is currently being used for understanding and control of the pyrolysis of polymers (see below). One critical requirement for the success of such modeling is the availability of a reliable database of rate coefficients of elementary reactions involved in the particular type of chemical processes being modeled. However, the existing database of gas-phase reaction rate coefficients primarily includes reactions involving relatively small molecules. Similarly, existing computational methods of predicting reaction rates have been developed and validated using experimental data for small-molecule reactions, as experimental data for gas-phase elementary reactions of large species are, generally, unavailable. As a result, modeling efforts directed at elucidation of such complex phenomena as the combustion of real fuels (relatively large long-chained, branched, and cyclic hydrocarbon molecules) and the pyrolysis of polymers are hindered by the lack of data on the rates of important elementary reactions. Nevertheless, modeling efforts continue, largely motivated by the need to develop computational tools of prediction and control, for both large hydrocarbon combustion (e.g., refs 1−4) and for the pyrolysis of polymers (e.g., refs 5−14 and references cited therein).

In the vast majority of the existing models of polymer pyrolysis, most of the rate coefficients used are derived from the corresponding gas-phase values of chemically similar but smaller species. One of the most important reaction types in polymer pyrolysis is the backbone scission, that is, the dissociation of the C−C bonds forming the polymer chain. These reactions are generally believed to be responsible for initiation of polymer pyrolysis. In evaluating the rate constants for polymer C−C bond dissociation, an approach based on an analogy with gas-phase small-molecule chemistry (decomposition of small alkanes) leads to preexponential factors of approximately $10^{16}-10^{17}$ s^{-1} and activation energy values close to the C−C bond strength, ∼ 348 kJ mol^{-1}. The deficiency of this approach becomes apparent when one compares the calculated temperature dependence of the rate constant with known experimental data on polymer pyrolysis. For example, the above Arrhenius parameters predict that the per-bond C−C bond scission rate constant, k_{CC}, will achieve the value of 1 s^{-1} at $T \cong 1070-1140$ K and that of 1×10^{-3} s^{-1} at $T \cong 910-960$ K. At the same time, the typical temperature range for the onset of polyethylene pyrolysis is 300−400 °C (573−673 K),[8,15] where the above Arrhenius parameters would give $k_{CC} \cong 2 \times 10^{-16}-1 \times 10^{-10}$ s^{-1}. Clearly, to explain the initiation of pyrolysis, rate constants of C−C bond scission need to have much larger values (also, see a discussion of rate constants in ref 8).

In a recent reactive molecular dynamics study (RMD), Nyden et al.[16] observed surprisingly low values of activation energies for chain scission of three alkane-based polymers, polyethylene, polypropylene, and polyisobutylene. These simulations were conducted under the conditions of polymer melt; the reactive force field used included several types of elementary reactions, including C−C backbone scission. The activation energy values obtained from the temperature dependences of the observed rate constant values were in the 40−190 kJ mol^{-1} range, which is much lower than the above typical value of the C−C bond strength. Furthermore, in a related RMD study of polyisobutylene (PIB) pyrolysis, Stoliarov et al.[17] demonstrated that the activation energy of the C−C scission decreases with the increased size of the polymer model. These authors reported

† Part of the special issue "James A. Miller Festschrift".

10.1021/jp066419e CCC: $37.00
Published on Web 04/14/2007

that the activation energy for C−C scission decreased from 239 kJ mol^{-1} in PIB-4 to 170 kJ mol^{-1} in PIB-150 (here and below, the number in the polymer notation is that of the monomer units that form the polymer chain).

Evaluation of the values and the temperature dependences of k_{CC} under the conditions of polymer melt requires a detailed analysis of all factors that may contribute to acceleration of the reaction relative to the case of small alkanes in the gas phase. To analyze and understand the overall result, each of the factors needs to be considered separately. The current study concentrates on the effect of the length of the alkane chain on the rates of C−C scission. To isolate the effect under study from other influencing factors, simulations in the current work are conducted for isolated molecules in the gas phase rather than in bulk polymer melt. Accordingly, in addition to the problem of polymer pyrolysis, these simulations are relevant to the combustion of long-chain hydrocarbons, major components of gasoline, kerosene, and diesel fuel.

Computational treatment of reactions of long-chain molecules in the gas phase via transition state theory (TST) is rather problematic. In the most widely used formulation of TST, partition functions of the reacting molecules and transition states are calculated assuming separability of all degrees of freedom, that is, these functions are obtained as products of partition functions of harmonic oscillators and one- and two-dimensional rigid rotors. Separability of rotational degrees of freedom has been confirmed for flexible-chain molecules of sizes up to pentane.[18] However, longer chains, especially those with the capability of coiling, have not been considered. Moreover, vibrational frequencies differ for different internal rotational conformations; the corresponding differences in vibrational partition functions are likely to increase with increasing chain length due to accumulation of differences caused by individual torsional angle changes. These effects are likely to result in coupling (nonseparability) of rotational and vibrational degrees of freedom and consequential difficulties in evaluating partition functions. In addition, use of TST in reactions of long-chain molecules is hindered by the presence of many very-low-frequency vibrational modes that cannot be treated as separable harmonic oscillators and have vibrational periods that may exceed the characteristic time of reaction.

Given the difficulties of applying TST to reactions of long-chain molecules, reactive molecular dynamics should be considered as a viable alternative for evaluation of reactivity. In the current study, reactive molecular dynamics modeling of C−C bond dissociation is performed for a series of linear alkanes and polyethylene macromolecules. The lengths of the alkane chain range from one to a thousand constituent monomers, PE-1−PE-1000. For PE-1−PE-5 chains, the rate constants obtained in molecular dynamics calculations are compared with those determined using variational transition state theory with the same potential energy surface and classical (as well as quantum) partition functions. The dependence of the per-bond C−C dissociation rates on the chain length are analyzed. The results of calculations are compared with existing experimental data on the dependences of the rates of thermal decomposition of linear alkanes on the alkane chain length.

2. Computational Methods

2.1. Molecular Dynamics Calculations. Molecular dynamics (MD) calculations were carried out for isolated single molecules. Linear alkanes and polyethylene chains ranging in length from PE-1 to PE-1000 were studied (PE-1 is ethane, PE-5 is *n*-decane, etc.). Since the main purpose of the study was investigation of the hypothetical effects of chain length and not derivation of exact values of rate constants, rather simple potential energy surfaces (PES) given by the all-atom OPLS-AA force field[19,20] with C−C stretch terms replaced by the Morse function were used. MD calculations were performed using GROMACS program package, version 3.2.[21,22] Initial linear structures of molecules were obtained by potential energy minimization. For each alkane/polyethylene molecule, a series of 10−40 calculations was performed at each temperature. In each such calculation, prior to the simulation of reactive events, a nonreactive simulation of molecular dynamics was performed for a period of 100−300 ps using harmonic C−C bond stretch terms to achieve randomization of molecular structures and atomic velocities. The resultant atom coordinates and velocities were used as the initial in subsequent reactive simulations. The Morse function parameters used in the reactive simulations were derived from those of the OPLS-AA harmonic force field by using the same equilibrium C−C distance and the second derivative of the potential at this distance. The bond dissociation energy used for all C−C bonds was 348 kJ mol^{-1}. The time integration step size of 0.2 fs was used in the simulations. Calculations were performed to demonstrate that increasing the time step by up to a factor of 5 (to 1.0 fs) did not produce any detectable changes in the calculated rate constant values. Overall translational motion of the center of mass and rotation around the center of mass were removed in all calculations.

Each MD calculation was continued until one carbon−carbon bond dissociated; the time required to achieve dissociation (t) was recorded. The value of t was averaged over 10−40 trajectory runs to obtain $<t>$, and the value of the rate constant was obtained as the inverse of $<t>$; the per-bond rate constant k_{CC} was calculated by further dividing by the number of bonds in the chain. Separation of the two carbon atoms forming a bond by the distance of 0.6 nm was used as the criterion of bond dissociation. Although this choice of the critical separation is rather arbitrary, selecting a different value would have only a negligible effect on the calculated rate constants as only very few cases of trajectories recrossing the dividing point were observed. To confirm the independence of the resultant rate constants of the C−C bond separation criterion, calculations were also performed for selected chain lengths and temperatures using the same trajectories but with the critical bond distance taken as 0.5, 0.8, and 1.0 nm. The results of such calculations using different bond dissociation criteria (presented in the Supporting Information, Table 1S) differ from those obtained with the original bond dissociation criterion by less than 14%. Temperatures used in modeling ranged from 2100 to 3000 K; such high temperatures were necessary to make the MD reaction rates observable within the practicable range of times of molecular dynamics simulations.

Temperature Control. Two methods were used for temperature control in MD simulations, those of Nose−Hoover[23,24] and Berendsen et al.[25] For small molecules (PE-25 and smaller), only the Nose−Hoover method was used. The resultant distributions of internal energies were analyzed and were found to coincide with the Boltzmann distributions calculated using vibrational frequencies of the species involved (e.g., Figure 1). However, for large molecules (PE-250 and larger), use of the Nose−Hoover algorithm of temperature control resulted in nonphysical oscillations of temperature. Thus, the Berendsen method was used for large chains. Calculations were performed to demonstrate that the rate constants obtained in simulations did not depend on the method of temperature control

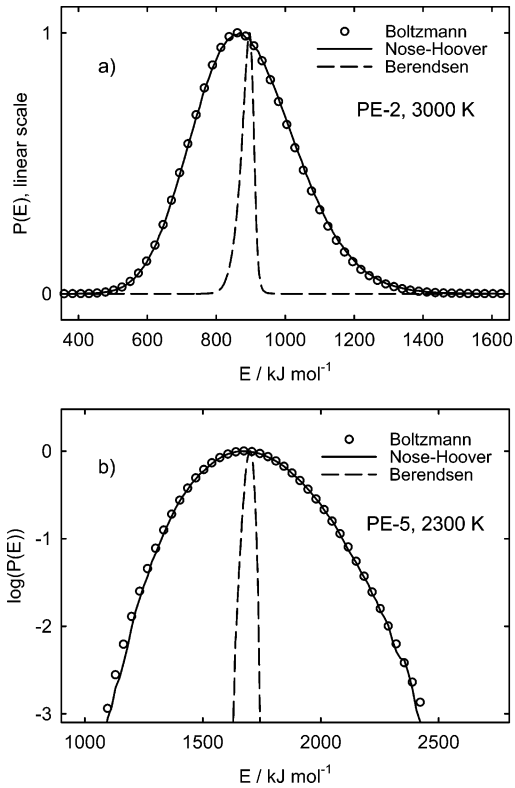

Figure 1. Examples of distributions of internal energy obtained in MD simulations using two different methods of temperature control (lines) in comparison with the classical (nonquantum) Boltzmann energy distributions calculated using vibrational frequencies of the corresponding molecules.

for chains of PE-25 and larger (see Table 2S in the Supporting Information).

This independence of the bond dissociation rates on the method of temperature control can be explained by considering the energy distributions resulting from the use of these two algorithms and from expressions for the unimolecular rate constant obtained in classical (nonquantum) versions of the transition state theory (TST) and the RRKM theory,[26−29] which is a microcanonical version of TST. The Nose−Hoover temperature control algorithm results in a Boltzmann distribution of internal energies[24,30] (also see Figure 1), and thus, the corresponding simulations are best represented by a TST expression for a canonical (fixed temperature) ensemble. The Berendsen algorithm analyzes the kinetic energy of the system at each time step of the trajectory integration and utilizes a velocity rescaling scheme that forces the system to a set value of temperature (and thus to a set value of the total kinetic energy). Deviations from the set value of temperature are corrected not immediately but with a rate determined by a preselected coupling time constant τ. Due to an approximate equidistribution of the kinetic and the potential energies in a system dominated by harmonic or almost harmonic potentials, maintaining a set value of the total kinetic energy with a characteristic time constant that is significantly longer than the typical vibrational period results in an approximate preservation of the average total energy of the system. The resulting energy distribution, although not an ideal δ-function, is nevertheless significantly more narrow than the Boltzmann distribution corresponding to the same temperature, as illustrated by plots in Figure 1.

To analyze the differences in the rate constants that can be expected to result from the use of these two methods of temperature control, one can consider unimolecular reaction rate constants given by the canonical and the microcanonical versions of the transition state theory. These two versions of TST represent two qualitatively limiting cases of the shapes of the total internal energy distributions: on one end, the Boltzmann distribution (canonical TST, fixed temperature) and on the other end, a δ-function distribution (microcanonical TST or RRKM,[26−29] fixed total energy). For such a comparison to be meaningful, the total energy used in the RRKM calculations should be taken as equal to the average total energy of the Boltzmann distribution at the temperature used in canonical TST calculations. Molecular dynamics simulations performed using the Nose−Hoover temperature control algorithm result in a Boltzmann distribution of the total internal energy and thus are best associated with the canonical TST approach. Those performed using the Berendsen algorithm, however, yield energy distributions that are much more narrow and are closer to the case of a fixed total energy (microcanonical TST or RRKM). Since the Berendsen energy distribution, although narrow, is still not an ideal δ-function, the difference between RRKM and canonical TST can be expected to be larger than that between the Nose−Hoover and the Berendsen temperature control methods. Thus, if an equivalence can be shown between the rate constants resulting from the canonical TST and from the RRKM method, this would mean that molecular dynamics simulations utilizing the Nose−Hoover and the Berendsen temperature control methods can also be expected to yield similar values of the rate constants.

The transition state theory expression[31] for the rate constant at temperature T is

$$k = \frac{k_B T}{h} \frac{Q^{\ddagger}}{Q} \exp\left(-\frac{E_0}{k_B T}\right) \qquad \text{(I)}$$

where $Q^{\ddagger}$ and Q are the partition functions of the transition state and the molecule, respectively, h is the Planck constant, E_0 is the reaction energy barrier, and k_B is the Boltzmann constant. Considering a molecule with n vibrational degrees of freedom and a corresponding transition state with $n-1$ degrees of freedom and using classical expressions[26,28] for the vibrational partition function

$$Q_{VIB} = \frac{k_B T}{h\nu} \qquad \text{(II)}$$

(ν is the vibrational frequency), one obtains

$$k_{TST} = \tilde{\nu} \exp\left(-\frac{E_0}{k_B T}\right) \qquad \text{(III)}$$

where

$$\tilde{\nu} = \frac{\prod_{i=1}^{n} \nu_i}{\prod_{i=1}^{n-1} \nu_i^{\ddagger}} \qquad \text{(IV)}$$

and ν_i and $\nu_i^{\ddagger}$ are vibrational frequencies of the molecule and the transition state, respectively.

The RRKM energy-dependent rate constant for the same reaction equals

$$k_{RRKM} = \frac{W^{\ddagger}(E)}{h\rho(E)} \qquad \text{(V)}$$

where $W^{\ddagger}(E)$ and $\rho(E)$ are the sum of states of the transition state and the density of states of the molecule, respectively.[26,28,29] Taking classical expressions[26,28] for these functions

$$W^{\ddagger}(E) = \frac{(E - E_0)^{n-1}}{(n-1)! \prod_{i=1}^{n-1} h\nu_i^{\ddagger}} \quad \text{(VI)}$$

$$\rho(E) = \frac{E^{n-1}}{(n-1)! \prod_{i=1}^{n} h\nu_i} \quad \text{(VII)}$$

and using total energy $E = nk_BT$ (average total energy of the Boltzmann distribution at temperature T), one obtains

$$k_{RRKM} = \frac{W^{\ddagger}(E)}{h\rho(E)} = \tilde{\nu}\left(1 - \frac{E_0}{nk_BT}\right)^{n-1} \quad \text{(VIII)}$$

For sufficiently large molecules, $nk_BT \gg E_0$; using Taylor series expansion for expression VIII, one obtains

$$\ln\left(\frac{k_{TST}}{k_{RRKM}}\right) = -\frac{E_0}{nk_BT} + \frac{n-1}{2}\left(\frac{E_0}{nk_BT}\right)^2 + \frac{n-1}{3}\left(\frac{E_0}{nk_BT}\right)^3 + \ldots \quad \text{(IX)}$$

The limit of expression IX at $n \rightarrow \infty$ is zero, and thus, for sufficiently large molecules, the differences between the rate constants obtained in the cases of canonical and microcanonical ensembles should disappear. Numerical evaluation of expressions III and VIII demonstrates that the differences between k_{TST} and k_{RRKM} are already less than 6% for PE-25 at 2000 K.

The above comparison of the rate constants of unimolecular decomposition obtained in the two limiting cases of wide (Boltzmann) and narrow (δ-function) distributions of internal energy demonstrate that these rate constants converge for large molecules possessing sufficient numbers of degrees of freedom. As discussed above, this convergence provides an explanation for the equivalence of the rate constants obtained in MD simulations of C−C bond scission in linear PE chains (PE-25 and longer) using two methods of temperature control, those of Nose−Hoover and Berendsen et al.

The time constant for temperature coupling (in the Berendsen algorithm) and the period of oscillation of kinetic energy between the molecule and the heat reservoir (for the Nose−Hoover algorithm) used were equal to 0.5 ps. Computations were performed to demonstrate that increasing or decreasing these time constants by an order of magnitude did not result in any detectable changes in the rate constants.

Calculations using Modified Hamiltonians. In addition to calculations using the OPLS-AA[19,20] force field, several series of MD simulations were performed for PE-5 using modified Hamiltonians, corresponding to "freezing" or impeding various degrees of freedom. In one series, all C−C bonds except for the central one were constrained to their corresponding equilibrium distances. In the second series, all C−C−C angles were partially frozen by increasing the corresponding force constants by a factor of 1000. In the third series, all angle potential terms (C−C−C, H−C−H, and C−C−H) were partially frozen by increasing the corresponding force constants by a factor of 100. In the fourth series, all C−C−C−C torsions were partially frozen by increasing the force constants by a factor of 1000. Due to software limitations, only in the first series (frozen C−C bonds) were full constraints implemented; in other series, the corresponding degrees of freedom could be restrained only by increasing the force constants.

2.2. Transition State Theory Calculations. The variational transition state theory (VTST) calculations of the C−C dissociation rate constants were performed for decomposition of four molecules, PE-1 ($C_2H_6 \rightarrow CH_3 + CH_3$), PE-2, PE-3, and PE-5. All channels of possible C−C bond scission were analyzed for these molecules. The canonical variational transition state theory approach[28,29,32,33] was used to obtain the rate constant values, that is, at each temperature, the C−C separation distance corresponding to the lowest value of the calculated rate constant was determined, and this lowest k_{CC} value was accepted for this temperature. Classical (nonquantum) partition functions for vibrational degrees of freedom and for hindered internal rotations were used in all VTST calculations to maintain compatibility with MD modeling, which is inherently classical.

All calculations of the potential energy surface properties were performed using the Gaussian 03 program package.[34,35] Potential energy profiles were obtained as functions of the C−C separation distances; at each constrained C−C separation, optimization of all of the internal coordinates corresponding to the remaining degrees of freedom was performed. Vibrational frequencies for the modes orthogonal to the reaction path[36,37] were obtained from a harmonic analysis projecting out of the C−C separation coordinate. In a recent study of the PE-1 decomposition by Klippenstein et al.,[38] projected vibrational frequencies resulting from this approach (but with a more realistic and complicated potential energy surface obtained in high-level quantum chemical calculations) were demonstrated to be identical to those obtained via the reoriented optimized dividing surface method of Villa and Truhlar,[39] which was developed by these authors to enable variational TST calculations without obtaining a converged minimum-energy path. For the calculations performed in the current work, parameters of the AMBER force field[40] included in Gaussian 03 were modified to most closely match those of the OPLS-AA force field. After this modification, the only difference between the AMBER and the OPLS-AA representations of the PES of the considered reactions was in the torsional potentials, which are described with the use of different functional forms in these two force fields. These differences, however, have no consequences for the values of rate constants, as explained below.

The classical partition function $Q_{HR}(T)$ of a one-dimensional hindered rotor can be expressed as[18,41,42]

$$Q_{HR}(T) = \tilde{Q}_{ROT}(T)\tilde{Q}_{SH}(T) \quad \text{(X)}$$

where T is the temperature, $\tilde{Q}_{ROT}(T)$ is the partition function of the corresponding free rotor (i.e., the same rotor without the hindering potential), and

$$\tilde{Q}_{SH}(T) = \frac{1}{2\pi}\int_0^{2\pi} d\xi \exp\left(-\frac{V(\xi)}{k_BT}\right) \quad \text{(XI)}$$

Here, the $\tilde{Q}_{SH}(T)$ term is determined by the shape of the hindering $V(\xi)$ potential (ξ is the torsional angle). In each of the reactions of decomposition of PE-1−PE5, the transition state and the molecule undergoing decomposition have the same number of internal hindered rotors. Moreover, the same functions describe the torsional hindering potentials in the transition state and in the molecule because the torsional force field parameters in AMBER and OPLS-AA do not change with the C−C distance. Thus, in the transition state theory expression for the rate constant (equation I), the $\tilde{Q}_{SH}(T)$ components of

TABLE 1: Per-Bond Rate Constants of C−C Scission Obtained in MD and TST Calculations

	Rate Constants (k_{CC}/s^{-1}) and Relative Uncertainties[a]				
alkane	2100 K	2300 K	2500 K	2700 K	3000 K
			MD Calculations		
PE-1		7.12×10^5(0.14)	1.43×10^6(0.19)	9.49×10^6(0.24)	3.78×10^7(0.26)
PE-2		1.20×10^6(0.18)	5.79×10^6(0.28)	1.56×10^7(0.21)	8.34×10^7(0.29)
PE-3		2.24×10^6(0.15)	7.07×10^6(0.13)	2.92×10^7(0.15)	1.18×10^8(0.11)
PE-5	9.48×10^5(0.28)	3.88×10^6(0.14)	1.86×10^7(0.12)	4.65×10^7(0.15)	2.57×10^8(0.14)
PE-25	6.51×10^5(0.23)	7.31×10^6(0.21)	1.99×10^7(0.18)	5.68×10^7(0.17)	
PE-100	1.44×10^6(0.24)	5.85×10^6(0.36)	1.70×10^7(0.26)	5.97×10^7(0.28)	
PE-250	1.20×10^6(0.22)	8.02×10^6(0.17)	2.36×10^7(0.22)	6.18×10^7(0.18)	
PE-1000	1.20×10^6(0.18)	4.44×10^6(0.30)	2.03×10^7(0.28)	7.58×10^7(0.28)	
			Classical VTST Calculations		
PE-1	1.06×10^5	5.91×10^5	2.49×10^6	8.49×10^6	3.93×10^7
PE-2	2.30×10^5	1.30×10^6	5.55×10^6	1.91×10^7	8.98×10^7
PE-3	3.83×10^5	2.13×10^6	8.99×10^6	3.06×10^7	1.41×10^8
PE-5	4.80×10^5	2.68×10^6	1.13×10^7	3.86×10^7	1.78×10^8

[a] Relative uncertainties (1σ uncertainty divided by the k_{CC} value) are given in parentheses.

the rotational partition functions will cancel in the $Q^{\ddagger}/Q$ ratio (the ratio of the partition functions of the transition state and the molecule). As a result, the rotational component of the $Q^{\ddagger}/Q$ ratio will be given by the ratios of partition functions of free one-dimensional rotors, that is, the ratios of the square roots of the corresponding moments of inertia.[26,28,29]

VTST calculations were performed for the case of zero angular momentum, that is, partition functions of the two-dimensional overall rotational degrees of freedom of the molecule and the transition state were not included in the calculation of the rate constant (see refs 26−29 for a discussion of active and adiabatic rotations). This was done to maximize the similarity to MD simulations, in which overall rotations of the molecule as a whole were removed. Reduced moments of inertia of the one-dimensional internal rotations were calculated using the method of Pitzer and Gwinn.[41,43] Contributions of the vibrational partition functions were calculated using equation II. Individual values of the projected vibrational frequencies and rotational constants are given in the Supporting Information (Table 3S) for selected individual reactions at selected C−C separations.

Linear extended chain structures with 180° C−C−C−C dihedral angles were used for all molecules and transition states. Effects of using partially coiled structures (e.g., with several C−C−C−C dihedral angles equal to ∼60°) were evaluated. Besides models in which torsional degrees of freedom were treated as hindered one-dimensional rotors, rate constant were calculated with models in which torsions were treated as harmonic oscillators. This was done to enable comparison between rate constants obtained for linear and partially coiled structures because identification of vibrational modes corresponding to torsions is rather complicated for nonlinear chain structures. Visual identification is easily performed for the linear configuration using normal mode animation. However, in cases of nonlinear configurations, many vibrational modes resulting from normal-mode analysis cannot be unambiguously assigned to particular types of motion. In addition to classical VTST calculations, quantum vibrational partition functions were calculated, and the resulting rate constant values were compared to those obtained using purely classical models.

Variational effects in the reactions of C−C bond dissociation in PE-1−PE-4 and PE-5 are relatively weak. For example, for PE-1 decomposition at 2000 K, the optimized C−C distance corresponding to the minima of the k_{CC} versus T dependences changes from 0.46 nm at 1000 K to 0.44 nm at 3500 K; ignoring this dependence of the optimized C−C distance on temperature and fixing the transition state C−C distance at 0.46 nm would result in a less than 3% change in the rate constants at $T \geq 1000$ K. For the PE-5 → 2 C_5H_{11} reaction channel, fixing the transition state C−C distance at 0.48 nm would result in less than a 3% change in k_{CC} in the same temperature range and in a 35% change at 300 K. This relative unimportance of variational effects is caused by the artificial potential energy surface used, that of the AMBER/OPLS-AA force fields, in which bending force constants do not decrease with increasing C−C separation. Use of more realistic potential energy surfaces leads to significant variational effects, as demonstrated, for example, in refs 38 and 44. However, in the current work, use of the AMBER/OPLS-AA potential energy surface is essential to maintain comparability with the results of molecular dynamics simulations.

TABLE 2: Arrhenius Parameters[a] for Per-Bond Rate Constants of C−C Scission Obtained in MD and TST Calculations

alkane	log(A/s^{-1})	E_0/kJ mol^{-1}
	MD Calculations	
PE-1	13.52 ± 0.92	342 ± 46
PE-2	13.86 ± 0.27	342 ± 13
PE-3	13.82 ± 0.31	331 ± 15
PE-5	14.02 ± 0.23	325 ± 11
PE-25	14.48 ± 0.89	344 ± 40
PE-100	13.30 ± 0.28	288 ± 13
PE-250	13.76 ± 0.47	306 ± 22
PE-1000	14.17 ± 0.43	327 ± 19
	Classical VTST Calculations	
PE-1	13.59	344
PE-2	14.00	347
PE-3	14.14	346
PE-5	14.24	344

[a] $k_{CC} = A \exp(-E_0/RT)$ s^{-1}. Error limits are 1σ of the fit.

3. Results

Molecular dynamics modeling results demonstrate that alkane chain length has a pronounced effect on the rate of backbone C−C dissociation. Significantly faster backbone scission (in terms of rate constants expressed per C−C bond, k_{CC}) was observed for longer molecules. These results are presented in Tables 1 and 2 and in Figure 2, along with the results of VTST calculations. As illustrated in Figure 3, the dependence of k_{CC} on the chain length N in PE-N displays a fast growth at low N ($N = 1-5$) and saturation at larger N values ($N = 25-1000$). On average, MD rates of C−C bond dissociation of long-chain molecules ($N > 5$) are ∼10 times larger than those of ethane.

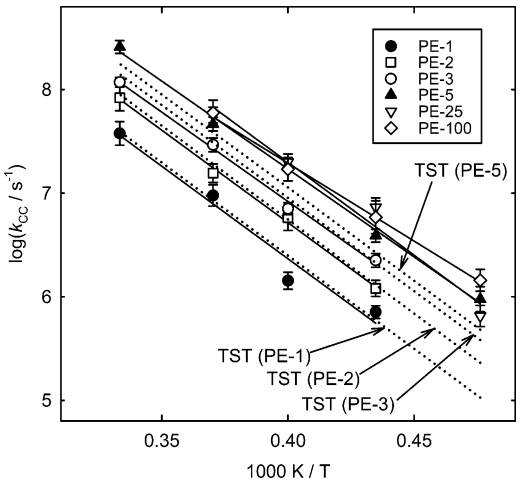

Figure 2. Per-bond rate constants k_{CC} for C−C backbone scission obtained in VTST (dotted lines) and MD (symbols and fitted solid lines) simulations. The plot shows the effect of chain length; rate constants increase with the increasing chain length. This dependence is saturated for polyethylene chains longer than PE-5. Rate constants obtained for PE-250 and PE-1000 are not shown to avoid plot congestion.

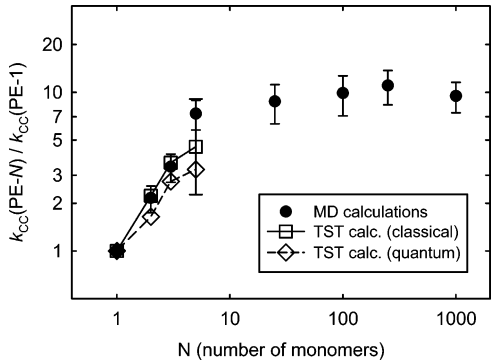

Figure 3. Dependence of the factor of acceleration of the C−C bond scission reactions (the average ratio of the per-bond rate constants obtained in simulations of PE-*N* decomposition to those of PE-1) on the alkane or polyethylene chain length. VTST rate constants are not calculated for $N > 5$ because of large uncertainties (see text). The estimated uncertainty of classical VTST calculations is shown for PE-5 only.

Transition state theory also predicts a noticeable increase in the dissociation rate constant with increasing chain length (Tables 1 and 2 and Figures 2 and 3). Per-bond rate constants increase in the PE-1−PE-5 sequence, in approximate agreement with the MD results. VTST results for PE-1 (ethane) agree with those obtained in MD calculations; the k_{CC}(T) dependences coincide (Figure 2). VTST rate constants for PE-5 decomposition are a factor of 4.5 larger than those for PE-1; the corresponding PE-5 versus PE-1 acceleration factor obtained in MD calculations is 7.3 (Figure 3). Purely vibrational TST models in which torsions were treated as harmonic oscillators yielded rate constants that are very close to those obtained using vibrational−rotational models, with differences of 0−16% over the 1000−3500 K temperature range for PE-1−PE-5. The observed agreement between the vibrational−rotational and the purely vibrational models is expected because of the similarity of the parameters of torsional degrees of freedom in the decomposing molecules and the corresponding transition states (see above). Rate constants obtained in quantum TST calculations (vibrational models) differed from the results of classical calculations by less than 16%.

Calculations performed with partially coiled PE-5 molecules indicate noticeable effects of torsional conformations on the TST rate constants. For example, rate constants obtained for the PE-5 → n-C_7H_{13} + n-C_3H_7 channel using a configuration of PE-5 that has six out of seven C−C−C−C dihedral angles equal to approximately 60° (spiral-like shape of the molecule) are a factor of 2.0 larger than those obtained for a linear extended shape of the same molecule. Configurations with less coiling resulted in smaller rate constant differences. The observed dependence of the TST rate constants on torsional conformation of the decomposing molecule reflects coupling between vibrational degrees of freedom and those of internal rotations, that is, dependence of vibrational frequencies on torsional configuration. For example, the ratios of classical and quantum vibrational partition functions of the above-mentioned spiral conformation of PE-5 to those of the linear extended conformation are equal to 6.8 and 5.4, respectively. The 2.0 ratio of the TST rate constants of these two conformation can be taken as a rough measure of uncertainty in the TST rate constant for PE-5 caused by this nonseparability of degrees of freedom (illustrated with error bars for the PE-5 data point in Figure 3).

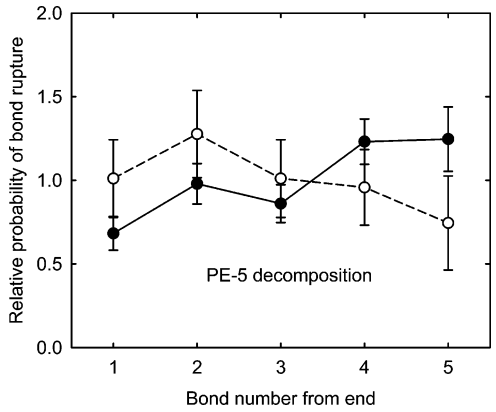

Figure 4. Dependences of the relative probability of bond scission on the bond position in the chain obtained in MD simulations of PE-5 decomposition using the "regular" force field (filled circles) and that with impeded torsions (open circles).

The Arrhenius fit parameters of the obtained k_{CC} temperature dependences are presented in Table 2. It is interesting to note that the temperature dependences of k_{CC} obtained in MD simulations are approximately parallel to each other on an Arrhenius plot (Figure 2). Thus, the reaction acceleration effects associated with the increasing chain length can be expressed in terms of increases in the preexponential factor, without noticeable changes in the values of the activation energy. All fitted activation energy values are close to the strength of the C−C bond used in the simulations, 348 k mol^{-1}.

The magnitude of the accelerating effect of the chain length was found to depend on the position of the dissociating bond in the chain. Figure 4 demonstrates that bonds located close to the molecule ends dissociate less often than those in the middle of the chain.

In an attempt to investigate the causes of the observed accelerating effects of molecular chain length, several series of MD simulations were performed using modified Hamiltonians in which certain types of degrees of freedom were constrained or impeded. The results of MD calculations with such modified Hamiltonians are presented in Figure 5. As can be seen from the plot, freezing C−C bond distances had no effects on the rate constants; the values of k_{CC} obtained in such calculations are similar to those obtained in "regular" PE-5, that is, larger than those in PE-1 by approximately a factor of 7. Partially freezing angles had some minor impeding effect on the C−C dissociation rates, although the magnitudes of these effects are

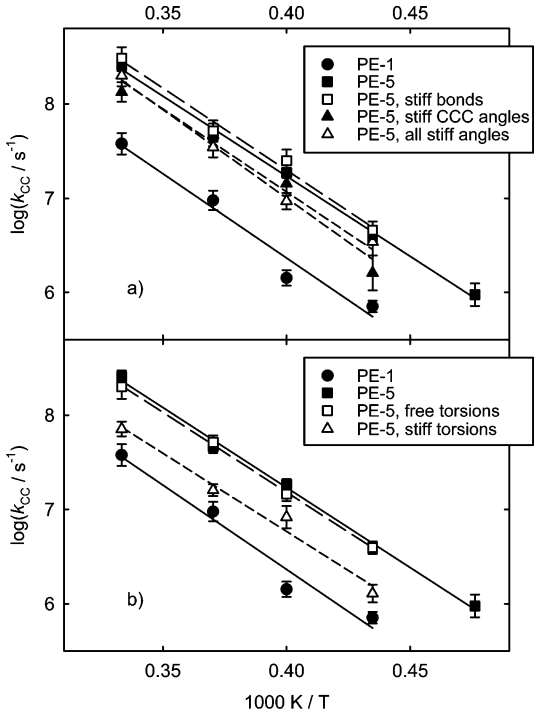

Figure 5. Per-bond rate constants k_{CC} for C−C backbone scission obtained in MD (symbols and fitted lines) simulations. The plot shows the effect of restrictions imposed on different types of motion in the decomposition of PE-5 (see text). MD-based rate constants for PE-1 (no reaction acceleration) are shown for comparison.

comparable with the estimated uncertainties in the rate constant values. The biggest effect was observed in the case of partially frozen C−C−C−C dihedral angles. The resultant rate constants are significantly lower than in the case of "regular" PE-5 and are closer to those observed in the case of PE-1. On the other hand, removing torsional barriers has no effect on the rate constants; the resultant rate constants coincide with those of the unaltered PE-5 model. It is also worth noting that the dependence of the probability of bond dissociation on its position (distance from the molecule end) observed in the case of the unmodified PE-5 Hamiltonian disappears when dihedral angles are partially frozen (Figure 4); no pronounced dependence exceeding the scatter of data within uncertainty limits can be observed in this case.

4. Discussion

The results of MD simulations performed in the current study demonstrate significant accelerating effects of chain length on the rates of C−C bond scission in linear alkanes. Per-bond rate constant values k_{CC} increase with the increasing chain length, up to a factor of 7.3, in the sequence of linear alkanes from PE-1 (ethane) to PE-5 (decane); this dependence becomes saturated for longer PE-*N* chain lengths (Figures 2 and 3), reaching an average value of the reaction acceleration factor (per-bond reaction rate relative to that of PE-1) equal to 10. Variational transition state theory (VTST) calculations performed using the same potential energy surface also predict an increase in the rate constant with increasing chain length. Classical and quantum VTST calculations yield per-bond reaction acceleration factors for PE-5 equal to 4.5 and 3.3, respectively.

Reaction acceleration observed in VTST calculations are caused by a general larger decrease in the values of projected vibrational frequencies of the transition states compared to those of the corresponding PE-*N* molecule with increasing chain length. Identification of the affected types of motion is not easy because of the considerable sizes of the molecules involved. For example, one cannot say, on the basis of visual analysis of animated vibrations, that transitional modes corresponding to rocking of the separating fragments are mainly responsible for the observed rate constant increases. VTST rate constants obtained in calculations using classical and quantum partition functions differ very little; both increase with the increasing chain length. This agreement between the rate constants versus chain length dependences obtained in quantum and classical calculations suggests that the observed positive trend is not an artifact of classical treatment.

Rate constant values obtained in VTST calculations become more uncertain with increasing chain length because of three major reasons. One reason is that projected vibrational frequencies become very small (as low as 20−30 cm^{-1} in transition states for PE-5 decomposition and even lower in longer chains) and the corresponding degrees of freedom cannot be treated as harmonic oscillators without a significant loss of accuracy. In addition, relative uncertainty of these projected frequencies obtained in practical numerical calculations increases beyond acceptable levels for chains longer than PE-5. The second reason is the increase in the number of potential internal rotational conformers of PE-*N* molecules and the corresponding transition states with increasing chain lengths, which grows as 3^N and introduces significant coupling between rotational and vibrational degrees of freedom, as described above. The third reason is the highly questionable separability of the rotational degrees of freedom in long-chain and coiling molecules, as discussed in the Introduction section. Because of accumulation of these uncertainties, use of VTST for chains longer than PE-5 becomes rather problematic; even for PE-5, the rate constant values have large uncertainties, as discussed above. For large molecules, using MD simulations provides a practicable alternative to TST calculations.

One implication of the findings of the current study is that, in modeling gas-phase chemical processes involving C−C bond scission of linear alkanes, such as the combustion of hydrocarbons, rate constants for such dissociation reactions need to be assigned with accounting for the effects of chain length. For example, the preexponential factor for the per-bond scission rate constant in *n*-decane can be expected to be approximately three times larger than that in *n*-butane, and so forth. Unfortunately, comparison of these predictions with experiment is problematic because existing experimental data on the decomposition of alkanes are sparse and have large uncertainties.[45] Most of the literature values of rate constants were obtained via final product analysis in flow tube experiments, where uncertainties of the temperature regimes, nonuniformity of heating, nonideal plug flow conditions, and potential effects of heterogeneous processes on the propagation/termination of chain reactions cause significant disagreements between the results of different groups of authors. In this respect, ratios of rate constants obtained for reactions of several different alkanes using the same apparatus and similar experimental conditions can be expected to be more reliable than the absolute rate constant values obtained in the same experiments.

The dependence of the preexponential factors of C−C bond scission in linear alkanes on the chain length has never been investigated in direct experiments. This is unlike the effects of methyl substitution at side chains, which have been studied and shown to exert no influence on the rate constants within experimental uncertainties.[46] However, the dependence of the

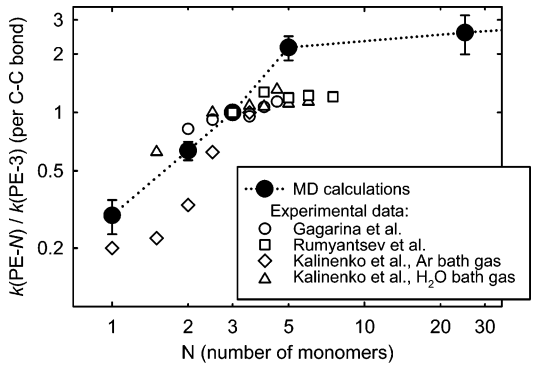

Figure 6. Comparison of the calculated dependence of the per-bond C−C scission rate constants on chain length (MD simulations) to the experimental dependences of the rates of thermal PE-*N* decomposition on *N*. Experimental data are from Gagarina et al.[47] (903−1010 K), Rumyantsev et al.[48] (873−993 K), and Kalinenko et al.[49] (913−1170 K). Reaction rates for PE-*N* are given relative to those of PE-3.

overall rates of thermal decomposition of linear alkanes on the chain length was studied experimentally by three groups.[47−49] These three studies used different but overlapping sets of linear alkane sizes; normal hexane (PE-3) was used in all of them. Figure 6 presents the results of these studies together with those of the MD modeling performed in the current work. All rates of alkane decomposition are put on the per-C−C-bond basis and are given relative to those of PE-3. As one can see from the plots in Figure 6, the general trend of the experimental data is the increase of the per-bond decomposition rate with increasing chain length at low *N* values and the tapering off of this dependence for longer chains. This general trend is in agreement with the results of the current MD study. It should be pointed out, however, that the above comparison between the MD predictions and the experimental results of refs 47−49 cannot be taken as providing a completely unambiguous experimental support for the computational results. Overall rates of alkane thermal decomposition depend not only on the rate constants of the initiation steps (C−C bond scission) but also on the rates of subsequent reactions of chain propagation and termination. Use of the same apparatus, experimental conditions, and method of analysis within each study is expected to eliminate some but not all of the variability factors.

Earlier, Nyden and Noid[50] studied dissociation of polyethylene macromolecules in the gas phase using molecular dynamics with Morse functions representing the potential of the C−C bonds. These calculations were performed for long chains only, PE-25−PE-500, using the united atoms approximation, that is, each CH_2 group was treated as one particle. The results of ref 50 did not indicate any dependence of the per-bond reactivity on the chain length within the used range of macromolecule sizes. The MD results of the current work indicate that the k_{CC} versus chain length dependence is saturated at these chain lengths. In this respect, the current results agree with the earlier findings of Nyden and Noid.

In a recent RMD study of polyisobutylene pyrolysis, Stoliarov et al.[17] demonstrated that the activation energy of the C−C scission decreases with the increased size of the polymer model, from 239 kJ mol^{-1} in PIB-4 to 124 kJ mol^{-1} in PIB-14, 189 kJ mol^{-1} in PIB-50, and 170 kJ mol^{-1} in PIB-150. Only calculations for PIB-4 were conducted for a single molecule in the gas phase; the rest of the PIB models included periodic boundary conditions to model bulk polymer melt. In the PIB-14, PIB-50, and PIB-150 sequence, the reduction of the activation energy coincided with the increase in the values of the per-bond rate constants. Since these results were obtained for the conditions of liquid polymer melt, they cannot be directly compared with those of ref 50 and the current work. The decrease in the activation energy with the increasing chain length observed in ref 17 is likely to be caused by phenomena that are different from those responsible for reaction acceleration with the increasing chain length in the PE-1−PE-5 range observed in the current study.

Investigation of the effects of restricting motion in different degrees of freedom in the reacting PE-5 chain demonstrated that impeding C−C stretches has no effect, impeding C−C−C as well as other bending motions has a relatively minor effect, and impeding C−C−C−C torsions has a rather significant decelerating effect on the reaction (Figure 5). The affected rate constants are still larger than those of PE-1 but are lower than those obtained for the unrestricted PE-5 model. Thus, impeding torsional degrees of freedom reduces the accelerating effect of the chain length. This importance of molecular torsions for the observed reaction acceleration effects may lead to a suggestion that coupling of internal rotations may be responsible for reaction acceleration in longer chains. Such coupling will result in nonseparability of the individual contributions of these degrees of freedom to the overall rotational partition functions. Any such nonseparability effect can be expected to increase with increasing chain length as the number of torsions also increases. However, any effects of nonseparability of rotational degrees of freedom on partition functions of long-chain molecules are likely to be similar in the transition state and in the decomposing molecule and thus will largely cancel in the TST expression for the rate constant (equation I). Thus, explanation of the observed reaction acceleration effects based on nonseparability of internal rotations seems unlikely.

As a working hypothesis, one can offer a different partial explanation for the observed acceleration of C−C bond scission in linear alkanes with increasing chain length. Torsional motions in the chain and, to a lesser extent, bending motions produce centrifugal forces that act on adjacent C−C bonds. These centrifugal forces result in quasiperiodic effective reductions or increases of the potential barriers for C−C bond dissociation as they are alternatively pulling the bonds apart or pressing the carbon atoms together. Since the dependence of the bond dissociation rate constant on the value of the energy barrier is heavily nonlinear, the averaged effect of these centrifugal forces is the increase in the rate constant. Increasing the chain length results in larger numbers of molecular motions producing centrifugal forces, which explains the observed increase in the rate constant with the chain length. On the other hand, longer chains tend to coil, which results in randomization of the directions of centrifugal forces (examples of trajectory snapshots showing approximate degrees of coiling are given in the Supporting Information, Figure 1S). Thus, for each C−C bond, only several adjacent torsions and bends affect the probability of dissociation, hence, the saturation of the rate constant versus chain length dependence. The observed lower probability of dissociation of terminal bonds (Figure 4) is thus explained by the smaller number of torsions and bends that can affect these bonds. Excitation of torsional and bending degrees of freedom increases with temperature, which in turn results in larger effective barrier lowering at higher temperatures; thus, the reaction accelerating effects of chain length do not decrease with temperature as they would in the case of energy barrier reduction by a constant value.

It is worth noting that the force field parametrization used in MD modeling performed in the current work is not without fault. One feature of such a force field that immediately draws

attention as physically unrealistic is that the force constants of bending degrees of freedom do not change with elongation of the constituent bonds. Although the resultant modeling cannot thus be expected to reproduce the effects of "loose" transition states of C−C bond dissociation (e.g., refs 51 and 28), this should not affect comparison of VTST- and MD-based rate constants because the same PES is used in both types of modeling. Similarly, the same force field is used for all chain lengths, from PE-1 to PE-1000; thus, the observed effects of chain length are not caused by differences in the PES representation.

The effects of chain length on the rates of C−C bond dissociation in linear alkanes observed in the current study may contribute to explanation of the experimental phenomenon of low-temperature pyrolysis of polymers (see Introduction). However, this can be only a partial explanation because the accelerating effects of chain length (up to an order of magnitude) are not sufficient to fully account for the known rates of polyethylene volatilization and the corresponding temperature of pyrolysis onset (e.g., refs 8 and 15 and references therein; also see a discussion of rate constants in ref 8).

Acknowledgment. This research was supported by the National Institute of Standards and Technology, Fire Research Grants Program, via Grant No. 70NANB4H1128. The author thanks Drs. M. R. Nyden and S. I. Stoliarov for stimulating discussions and Dr. T. C. Allison for help with the software. This study utilized the high-performance computational capabilities of the Biowulf PC/Linux cluster at the National Institutes of Health, Bethesda, MD. (http://biowulf.nih.gov).

Supporting Information Available: Selected detailed results of molecular dynamics calculations (Tables 1S−2S, Figure 1S) and those of geometry optimization and projected vibrational frequency calculations (Table 3S). This material is available free of charge via the Internet at http://pubs.acs.org.

References and Notes

(1) Bikas, G.; Peters, N. *Combust. Flame* **2001**, *126*, 1456.

(2) Humer, S.; Frassoldati, A.; Granata, S.; Faravelli, T.; Ranzi, E.; Seiser, R.; Seshadri, K. *Proc. Combust. Inst.* **2007**, *31*, 393.

(3) Dagaut, P.; Cathonnet, M. *Prog. Energy Combust. Sci.* **2006**, *32*, 48.

(4) Herbinet, O.; Marquaire, P. M.; Battin-Leclerc, F.; Fournet, R. *J. Anal. Appl. Pyrolysis* **2007**, *78*, 419.

(5) Kruse, T. M.; Wong, H.-W.; Broadbelt, L. J. *Macromolecules* **2003**, *36*, 9594.

(6) Kruse, T. M.; Wong, H.-W.; Broadbelt, L. J. *Ind. Eng. Chem. Res.* **2003**, *42*, 2722.

(7) Kruse, T. M.; Woo, O. S.; Wong, H.-W.; Khan, S. S.; Broadbelt, L. J. *Macromolecules* **2002**, *35*, 7830.

(8) Poutsma, M. L. *Macromolecules* **2003**, *24*, 8931.

(9) Faravelli, T.; Bozzano, G.; Colombo, M.; Ranzi, E.; Dente, M. *J. Anal. Appl. Pyrolysis* **2003**, *70*, 761.

(10) Faravelli, T.; Bozzano, G.; Scassa, C.; Perego, M.; Fabini, S.; Ranzi, E.; Dente, M. *J. Anal. Appl. Pyrolysis* **1999**, *52*, 87.

(11) Faravelli, T.; Pinciroli, M.; Pisano, F.; Bozzano, G.; Dente, M.; Ranzi, E. *J. Anal. Appl. Pyrolysis* **2001**, *60*, 103.

(12) Marongiu, A.; Faravelli, T.; Bozzano, G.; Dente, M.; Ranzi, E. *J. Anal. Appl. Pyrolysis* **2003**, *70*, 519.

(13) Madras, G.; McCoy, B. J. *Ind. Eng. Chem. Res.* **1999**, *38*, 352.

(14) Sterling, W. J.; Kim, Y.-C.; McCoy, B. J. *Ind. Eng. Chem. Res.* **2001**, *40*, 1811.

(15) Madorsky, S. L. *Thermal Degradation of Organic Polymers*; Wiley: New York, 1964.

(16) Nyden, M. R.; Stoliarov, S. I.; Westmoreland, P. R.; Guo, Z. X.; Jee, C. *Mater. Sci. Eng., A* **2004**, *365*, 114.

(17) Stoliarov, S. I.; Lyon, R. E.; Nyden, M. R. *Polymer* **2004**, *45*, 8613.

(18) Knyazev, V. D. *J. Phys. Chem. A* **1998**, *102*, 3916.

(19) Jorgensen, W. L.; Maxwell, D. S.; Tirado-Rives, J. *J. Am. Chem. Soc.* **1996**, *118*, 11225.

(20) Price, M. L. P.; Ostrovsky, D.; Jorgensen, W. L. *J. Comput. Chem.* **2001**, *22*, 1340.

(21) Lindahl, E.; Hess, B.; van der Spoel, D. *J. Mol. Model.* **2001**, *7*, 306.

(22) Berendsen, H. J. C.; van der Spoel, D.; van Drunen, R. *Comput. Phys. Commun.* **1995**, *91*, 43.

(23) Nose, S. *Mol. Phys.* **1984**, *52*, 255.

(24) Hoover, W. G. *Phys. Rev. A* **1985**, *31*, 1695.

(25) Berendsen, H. J. C.; Postma, J. P. M.; DiNola, A.; Haak, J. R. *J. Chem. Phys.* **1984**, *81*, 3684.

(26) Robinson, P. J.; Holbrook, K. A. *Unimolecular Reactions*; Wiley-Interscience: New York, 1972.

(27) Forst, W. *Theory of Unimolecular Reactions*; Academic Press: New York, 1973.

(28) Gilbert, R. G.; Smith, S. C. *Theory of Unimolecular and Recombination Reactions*; Blackwell: Oxford, U.K., 1990.

(29) Holbrook, K. A.; Pilling, M. J.; Robertson, S. H. *Unimolecular Reactions*, 2nd ed.; Wiley: New York, 1996.

(30) Allen, M. P.; Tildesley, D. J. *Computer Simulation of Liquids*; Oxford University Press: Oxford, U.K., 1987.

(31) Johnston, H. S. *Gas Phase Reaction Rate Theory*; The Ronald Press: New York, 1966.

(32) Truhlar, D. G.; Garrett, B. C. *Annu. Rev. Phys. Chem.* **1984**, *35*, 159.

(33) Truhlar, D. G.; Garrett, B. C.; Klippenstein, S. J. *J. Phys. Chem.* **1996**, *100*, 12771.

(34) Frisch, M. J.; Trucks, G. W.; Schlegel, H. B.; Scuseria, G. E.; Robb, M. A.; Cheeseman, J. R.; Montgomery, J. A., Jr.; Vreven, T.; Kudin, K. N.; Burant, J. C.; Millam, J. M.; Iyengar, S. S.; Tomasi, J.; Barone, V.; Mennucci, B.; Cossi, M.; Scalmani, G.; Rega, N.; Petersson, G. A.; Nakatsuji, H.; Hada, M.; Ehara, M.; Toyota, K.; Fukuda, R.; Hasegawa, J.; Ishida, M.; Nakajima, T.; Honda, Y.; Kitao, O.; Nakai, H.; Klene, M.; Li, X.; Knox, J. E.; Hratchian, H. P.; Cross, J. B.; Bakken, V.; Adamo, C.; Jaramillo, J.; Gomperts, R.; Stratmann, R. E.; Yazyev, O.; Austin, A. J.; Cammi, R.; Pomelli, C.; Ochterski, J. W.; Ayala, P. Y.; Morokuma, K.; Voth, G. A.; Salvador, P.; Dannenberg, J. J.; Zakrzewski, V. G.; Dapprich, S.; Daniels, A. D.; Strain, M. C.; Farkas, O.; Malick, D. K.; Rabuck, A. D.; Raghavachari, K.; Foresman, J. B.; Ortiz, J. V.; Cui, Q.; Baboul, A. G.; Clifford, S.; Cioslowski, J.; Stefanov, B. B.; Liu, G.; Liashenko, A.; Piskorz, P.; Komaromi, I.; Martin, R. L.; Fox, D. J.; Keith, T.; Al-Laham, M. A.; Peng, C. Y.; Nanayakkara, A.; Challacombe, M.; Gill, P. M. W.; Johnson, B.; Chen, W.; Wong, M. W.; Gonzalez, C.; Pople, J. A. *Gaussian 03*, revision C.02; Gaussian, Inc.: Wallingford, CT, 2004.

(35) Certain commercial instruments and materials are identified in this article to adequately specify the procedures. In no case does such identification imply recommendation or endorsement by NIST, nor does it imply that the instruments or materials are necessarily the best available for this purpose.

(36) Miller, H. W.; Handy, N. C.; Adams, J. E. *J. Chem. Phys.* **1980**, *72*, 99.

(37) Baboul, A. G.; Schlegel, H. B. *J. Chem. Phys.* **1997**, *107*, 9413.

(38) Klippenstein, S. J.; Georgievskii, Y.; Harding, L. B. *Phys. Chem. Chem. Phys.* **2006**, *8*, 1133.

(39) Villa, J.; Truhlar, D. G. *Theor. Chem. Acc.* **1997**, *97*, 317.

(40) Cornell, W. D.; Cieplak, P.; Bayly, C. I.; Gould, I. R.; Merz, K. M.; Ferguson, D. M.; Spellmeyer, D. C.; Fox, T.; Caldwell, J. W.; Kollman, P. A. *J. Am. Chem. Soc.* **1995**, *117*, 5179.

(41) Pitzer, K. S.; Gwinn, W. D. *J. Chem. Phys.* **1942**, *10*, 428.

(42) Knyazev, V. D.; Tsang, W. *J. Phys. Chem. A* **1998**, *102*, 9167.

(43) Pitzer, K. S. *J. Chem. Phys.* **1946**, *14*, 239.

(44) Klippenstein, S. J.; Harding, L. B. *J. Phys. Chem. A* **1999**, *103*, 9388.

(45) NIST Chemical Kinetics Database. Standard Reference Database 17, Version 7.0 (Web Version), Release 1.4. http://kinetics.nist.gov (accessed March 12, 2007).

(46) Tsang, W.; Kiefer, J. H. In *The Chemical Dynamics and Kinetics of Small Radicals*; Liu, K., Wagner, A., Eds.; World Scientific Publishing Co. Pte. Ltd.: Singapore, 1995; p 58.

(47) Gagarina, L. V.; Korzun, N. V.; Magaril, R. Z. *Izv. Vyssh. Uchebn. Zaved. Neft Gaz* **1982**, *25*, 42.

(48) Rumyantsev, A. N.; Shevel'kova, L. V.; Sokolova, V. M.; Nametkin, N. S. *Neftekhimiya* **1980**, *20*, 212.

(49) Kalinenko, R. A.; Buravtseva, E. N.; Nametkin, N. S.; Bach, G.; Zychlinskii, W.; Zimmermann, G. *Kinet. Catal.* **1983**, *24*, 873.

(50) Nyden, M. R.; Noid, D. W. *J. Phys. Chem.* **1991**, *95*, 940.

(51) Benson, S. W. *Thermochemical Kinetics*, 2nd ed.; John Wiley and Sons: New York, 1976.